Available online at www.sciencedirect.com
ScienceDirect
European Journal of Mechanics B/Fluids 25 (2006) 909–922

Basic flow characteristics in three-dimensional branching channel with sudden expansion

H. Yamaguchi [a,*], A. Ito [a], M. Kuribayashi [a], X.R. Zhang [a], H. Nishiyama [b]

[a] *Department of Mechanical Engineering, Doshisha University, Kyoto, 610-0321, Japan*
[b] *Institute of Fluid Science, Tohoku University, Sendai, 980-8577, Japan*

Received 7 June 2005; accepted 30 October 2005

Available online 14 February 2006

Abstract

Deflection characteristics of flows in three-dimensional branching channel geometries were obtained experimentally and phenomenological explanations were given by analyzing the three dimensional flow field numerically. It was found from the results of the experiments, which were verified by means of numerical simulation, that the defection characteristics are largely dependent upon the net contribution of the swirl component in the expanded channel part before entering each distribution outlet pipe. It was further revealed that there are different flow distribution characteristics when the distribution outlet pipes are further apart from the center of cylindrical axis in the expanded channel part.

Keywords: Three-dimensional cylindrical branching channel; Flow characteristic; Branch flow rate; Asymmetric flow

1. Introduction

Flows in pipelines and ducts are commonly encountered in many parts of fluid machineries, through which the transport of fluids, chemicals and other industrial or bio-medical liquids take place. These flows in many cases have to be delivered or distributed from a main line to a distribution network for specific purposes, such as often seen in hydraulic controls, heating and air conditioning systems, cardiovascular and pulmonary flow systems. In the situation of flow distribution or delivering system, pipe elements are often connected with constant-diameter piping and linked at junctions for distribution at network [1]. In addition, there has been a lot of work done in vascular flow that deals with branching geometry. For example, Liepsch [2] mentioned velocity distribution and hemodynamic forces acting on the vessel wall and blood cells are very important. Normally under physiological flow conditions, the flow is neither fully developed laminar flow nor turbulent flow. It can be described as laminar flow with periodically returning vortices. Liou et al. [3,4] studied experimentally pulsatile and steady flow in cerebrovascular aneurysm models with various sizes, bifurcation angles and volume-flow rate ratios. It is found that the vortex three-dimensional structure is main vascular flow characteristics and main cause of thinness of the aneurysm wall or aneurismal progression.

* Corresponding author.
E-mail address: hyamaguc@mail.doshisha.ac.jp (H. Yamaguchi).

0997-7546/$ – see front matter
doi:10.1016/j.euromechflu.2005.10.003

Nomenclature

E	expansion ratio	t^*	non-dimensionalized time
A_s	aspect ratio	u_i	radial velocity at P_i
D	diameter of the inlet pipe	u_i^*	non-dimensionalized radial velocity at P_i
d	diameter of the outlet branch pipes	v_i	circumferential velocity at P_i
L	axial length of the abruptly expanded part	v_i^*	non-dimensionalized circumferential velocity at P_i
l_0	the length of the inlet pipe and the outlet branch pipes	w_i	axial velocity at P_i
p	pressure	w_i^*	non-dimensionalized axial velocity at P_i
q_i	volume flow rate from each outlet branch pipe	V	total volume of the abruptly expanded part
		$W_{\max}$	maximum velocity in the inlet circular pipe
Re	Reynolds number	Γ_n	swirl ratio
r^*	non-dimensionalized radial distance	λ	flow rate distribution ratio
z^*	non-dimensionalized axial distance	ν	kinematic viscosity
t	time duration of the volume flow rate from each outlet branch pipe	ρ	density
		θ	circumferential angle

Flows in a symmetric channel configuration may deflect arbitrarily to one side along the symmetric axis of the channel. Here, the flow rate deflection is defined as the ratio of flow rate among outlet branch pipes. The phenomena are often treated as an instability problem [5,6] of flow, derived from the bifurcation theorem in non-linear differential equation system [7]. Cherdron et al. [5] investigated experimentally the velocity characteristics of the asymmetric flows which form in symmetric, two-dimensional, plane, sudden-expansion geometries. The reason for the asymmetric is shown to lie in disturbances generated at the edge of the expansion and amplified in the shear layers. A weakly nonlinear stability analysis [6] was used to study the structural instability of the bifurcation for flow in a symmetric channel with a sudden expansion. The steady symmetric and steady asymmetric flow regimes depending on the Reynolds number was shown, which is dependent on the expansion ratio. Fearn et al. [7] studied experimentally and numerically the origin of steady asymmetric flows in a symmetric sudden expansion. The obtained results showed that at higher Reynolds numbers, the flow becomes time-dependent and there is experimental evidence that this is associated with three-dimensional effects. The highest value of Re at which the flow remained steady was $Re = 151$ in the studied case. In addition, Alleborn et al. [8] and Hawa and Rusak [9] investigated two-dimensional flow in a sudden expansion, which demonstrated that when $Re > Re_c$, the symmetric mode becomes unstable. Experimental investigations [10,11] were described for the flow in symmetric or axisymmetric sudden expansion. The results showed that at the lower Reynolds numbers, the flow was very stable. At higher Reynolds numbers the flow becomes less unstable and periodicity became increasingly important in the main stream.

However literature review revealed that in spite of the importance in fluid engineering, there is only few published information, regarding flow distribution channels in practical uses. In the present study, a cylindrical manifold distribution channel with one inlet and two outlet pipes is considered. The channel has a three-dimensional geometric configuration with a sudden expansion at the inlet and sudden contraction at the outlet. Particularly in the present study, model channels with the expansion ratio of 3 and the aspect ratio of $7/3$ are adopted for two different outlet pipe positions, where the specification was often quoted as the bench mark channel [12,13] from view point of fundamental fluid mechanics, and has engineering significance in practice. This configuration is widely applied in chemical plants and plastic modeling processes, medical engineering and bioengineering. The important point of the configuration is the expansion ratio $(3/7)$ of the channel, which is so often quoted in references as the bench mark case. The outlet branch channels are rather arbitrary so that two representative cases are studied in this study. The present study involves local velocity measurements in the channels and flow visualization, associated with measurements of flow rate distribution characteristics from two outlet pipes in two different representative positions. Furthermore, in order to shed light onto the physics in the experiment work, a numerical analysis is carried out by using HSMAC (Highly Simplified Maker And Cell) method [14] in a three-dimensional flow domain.

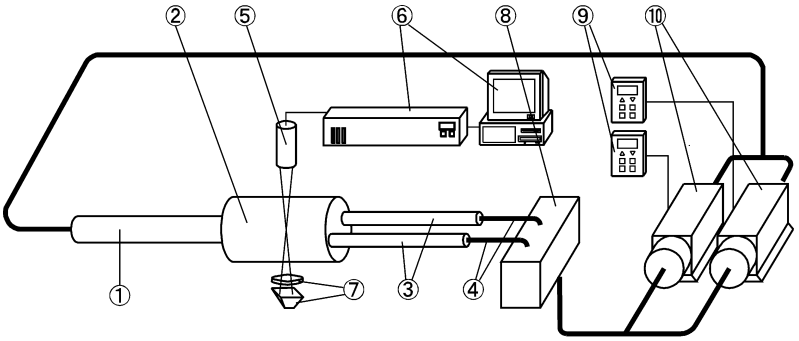

① Inlet pipe
② Abruptly expanded part
③ Outlet distribution pipes
④ Leading pipes
⑤ Laser Doppler Velocimeter
⑥ Data acquisition system
⑦ Corner cube reflection & condenser lense
⑧ Reservoir tank
⑨ Inverter controller
⑩ Gear pump

Fig. 1. Experimental apparatus.

2. Experimental apparatus and procedure

The summary of the experimental equipment is shown in Fig. 1. In the present experiment, working fluid (glycerin water solution) was circulated by two gear pumps in parallel arrangement. The working fluid was then sent to the inlet pipe of the test section. The test section (a cylindrical branching channel) consists of an inlet pipe, abruptly expanded part and two outlet branch pipes placed at the end of the abruptly expanded part. The details of the test sections are displaced in Fig. 2 (for two distinct outlet pipes positions; channel 1 and channel 2). The diameter of the inlet pipe is $D = 40$ mm, and the length of the inlet pipe and outlet pipes was chosen for the sufficient length, $l_0 = 1300$ mm from McComas's theory [15] ($l_0 = 0.0260\,Re\,D$), so that the flows at the inlet of the abruptly expanded part and at the outlet of each outlet branch pipe can be sufficiently developed as the Poiseuille pipe flow. The geometric configuration of the abruptly expanded part was chosen from a typical abrupt expansion system geometry; the expansion ratio E (diameter of the abruptly expanded part/diameter of the inlet pipe) is $E = 3$ and the aspect ratio A_s (axial length of the abruptly expanded part $L = 280$ mm/diameter of the abruptly expanded part $3D$) is $A_s = 7/3$. After entering the abruptly expanded part, the fluid was distributed to two identical outlet branch pipes. The diameter of the outlet branch pipes is $d = 20$ mm identically and the distances between central axes of the two outlet branch pipes are $3D/2$ and $3D - d$ for channel 1 and channel 2 respectively as shown in Fig. 2. It is mentioned that such three dimensional branching channels are widely utilized as a typical distributor in fluid engineering, and which can be thought and treated as bench mark cases in fundamental hydrodynamic research. The working fluid, after leaving two outlet branch pipes, was lead to the reservoir tank and was then circulated again by the two gear pumps. The whole test section was made of transparent acrylic resin material so that the velocity measurement and flow visualization are possible. In the present study, the cylindrical coordinate system of r (the radius coordinate), θ (the angle coordinate), and z (the axial coordinate) was used, whose origin 0 is set at the inlet of the abruptly expanded part as indicated in Fig. 2. In the present study, velocities at some representative points were measured [16] in order to test if the flow was steady or unsteady and to identify the asymmetric flow.

The working fluid used in the present investigation was glycerin water solution as mentioned previously, with which the inlet Reynolds number, $Re = W_{\max} D/\nu$, can be extended to $Re = 1000$, where ν is the kinematic viscosity and $W_{\max}$ the maximum velocity (axial velocity at the axis of pipe of Poiseuille flow) in the inlet circular pipe. It should be noted that throughout flow experiments temperature of the working fluid was monitored. The temperature variation was fined between 19–25 °C during whole experiments and the physical properties for Reynolds number were corrected in terms of temperature variation for each experiment.

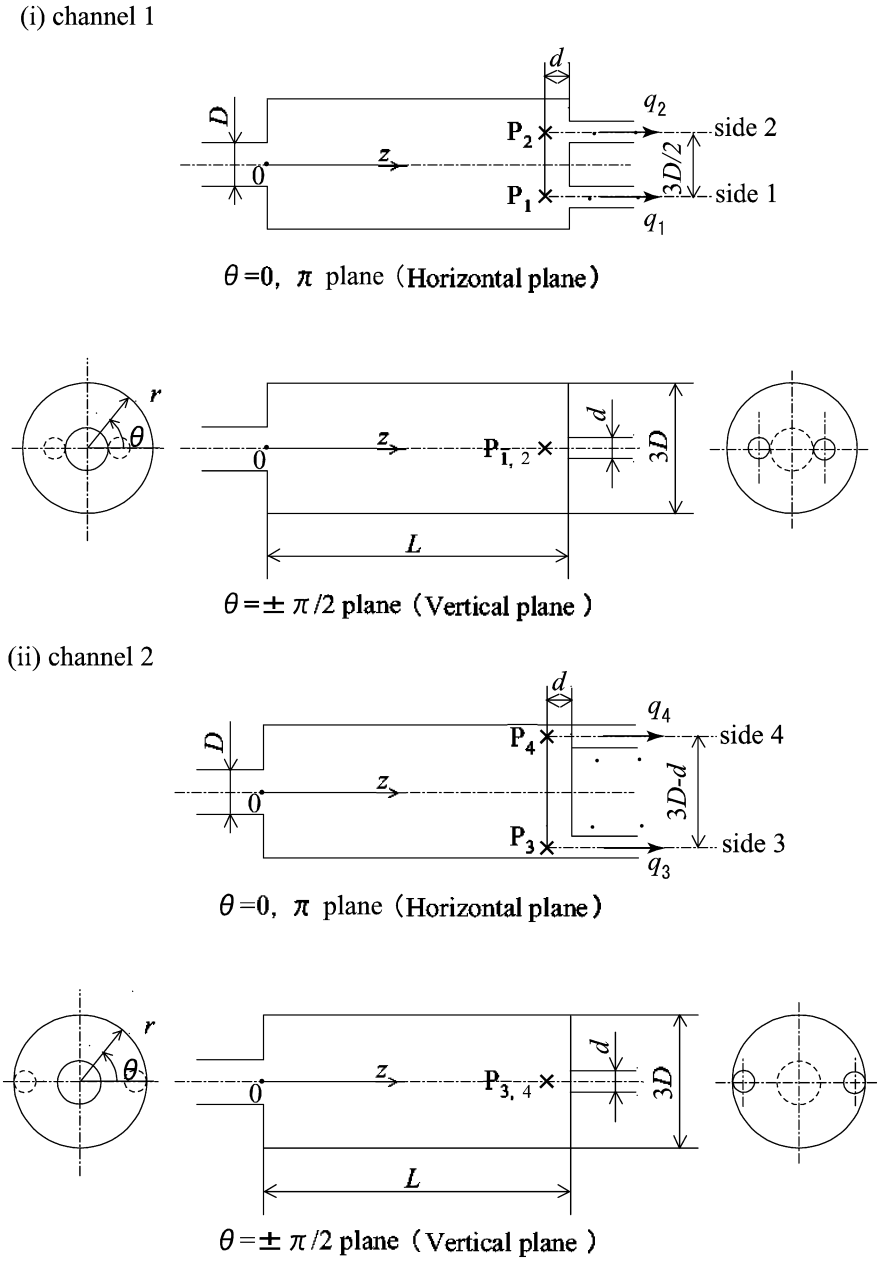

Fig. 2. Details of test section.

In the present experiment the volume flow rate from each outlet branch pipe was measured by collecting volume of flow for time duration of 5–15 seconds from each leading pipe to the reservoir tank. The volume flow rate q_1 and q_2 from each outlet branch pipe (as shown in Fig. 2) is then calculated by the following equations:

$$q_1 = m_1/\rho t, \qquad q_2 = m_2/\rho t \tag{1}$$

where m_1, m_2 are the weight of the working fluid collected from each outlet branch pipe, t is sampling time. The measurement of the volume flow rate was repeated at least five times and the average value was adopted. The measurement accuracy of the volume flow rate from each outlet branch pipe was found to be maximum $\pm 1\%$, which was estimated from deviation of each repeated data. The measurement details can be seen in Ref. [16].

Flow visualization was also achieved by mixing a little amount of aluminum oxide powder with a surfactant to the working fluid. The flow phenomena in the abruptly expanded part showed very complicated three-dimensional flow patterns so that in the present investigation flows in the horizontal plane; $\theta = 0, \pi$ plane and the vertical plane; $\theta = \pm\pi/2$ plane were observed by focusing slit light to the planes. The images of flows were recorded as still image by a high resolution digital camera.

3. Numerical analysis

In the present study, simulation of the incompressible Newtonian fluid was carried out in order to clarify the behavior of flow in the test sections.

The flow is assumed as incompressible and isothermal so that the flow field can be written by the continuity equation and Navier–Stokes equation as,

$$\nabla \cdot \boldsymbol{v}^* = 0, \tag{2}$$

$$\frac{\partial \boldsymbol{v}^*}{\partial t^*} + \left(\boldsymbol{v}^* \cdot \nabla\right)\boldsymbol{v}^* = -\nabla p^* + \frac{1}{Re}\Delta \boldsymbol{v}^* \tag{3}$$

where Eqs. (2) and (3) are in non-dimensional form. Parameters appearing in Eqs. (2) and (3) are defined as,

$$\boldsymbol{x}^* = \frac{\boldsymbol{x}}{D}, \quad \boldsymbol{v}^* = \frac{\boldsymbol{v}}{W_{\max}}, \quad p^* = \frac{p}{\rho W_{\max}^2}, \quad t^* = \frac{W_{\max}}{D}t, \quad Re = \frac{W_{\max} D}{\nu} \tag{4}$$

where $\boldsymbol{x} = (r, \theta, z)$ is the coordinate, $\boldsymbol{v} = (u, v, w)$ the velocity vector and p the pressure, ρ the density, t the time and ν the kinematic viscosity. As seen in Eq. (4), parameters appearing in Eqs. (2) and (3) are non-dimensionalized by D, diameter of the inlet circular pipe and $W_{\max}$, maximum velocity component at the axis of the inlet circular pipe.

The numerical solutions of the flow field were obtained by the Highly Simplified Maker and Cell method [14]. The discretization was done by the finite difference approximation, namely the second order central finite difference for the viscous diffusion terms, the third order up-stream finite difference for the convective terms and the first order forward finite difference for time derivative. The second-order scheme is used to handle the pressure term in the present study. In addition, an outflow flow boundary condition is used to model flow exists where the details of the flow velocity and pressure are not known prior to solution of the flow problem. In Fig. 3 (i) and (ii), representative mesh systems are displayed together with the cylindrical coordinate system and the definition of the vertical plane and horizontal plane for channel 1 and channel 2 respectively. Grid independence of the results was established by employing various number of mesh points, ranging from 100,000 to 1,296,000, but it was verified that the mesh configuration $15 \times 80 \times 135$ is the optimum. Further increase of mesh number did not yield further improvement of numerical precision. The grid independence was tested under the representative Reynolds number 100, 300, 400, 630, 800 and 1000 in the present geometry configuration. The mesh configuration $30 \times 160 \times 270$ made only maximum 0.3% difference in representative, such as the flow rate deflection and the re-attachment length at the abruptly expanded part.

Boundary conditions for flow field calculation are:

1. Before the entrance of the abruptly expanded part at $z^* = -2.5$, it is assumed that the flow is fully developed Poiseuille pipe flow and following Dirichlet conditions are given:

$$u^* = 0, \quad v^* = 0, \quad w^* = 1 - 4r^{*2}. \tag{5}$$

2. At the exit of each outlet branch pipe, at $z^* = 11$, the outlet flow condition is assumed as the fully developed flow and is given by following Neumann condition. In addition, a pressure outlet boundary condition was used in the numerical scheme. That is, gauge pressure was set as zero at the outlet.

$$\frac{\partial \boldsymbol{v}^*}{\partial z^*} = 0. \tag{6}$$

The mass conservation is the most important issue in this work. For inlet volumetric flow rate in incompressible flow, the continuity of mass (for constant density) is such that inlet volumetric flow rate equals to the volumetric flow rate from channel 1 and channel 2. In the numerical analysis, the condition is always monitored and ensured in each time step.

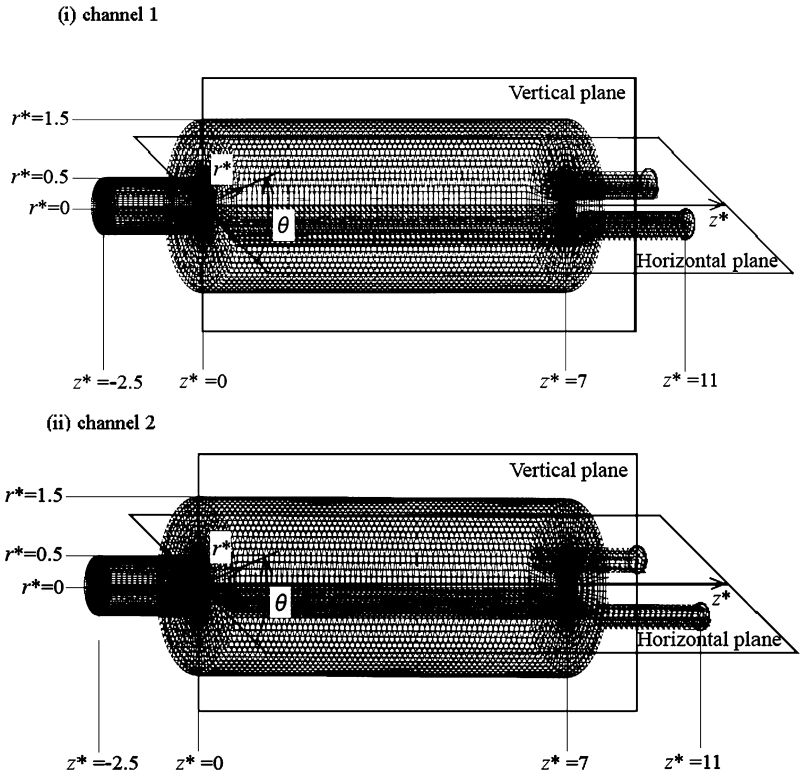

Fig. 3. Mesh system.

3. At every wall in the test section, non-slip flow condition is given by following Dirichlet conditions:

$$u^* = 0, \quad v^* = 0, \quad w^* = 0. \tag{7}$$

4. Particular attention was given at the axis of the test section, $r^* = 0$, where the singularity of numerical solution occurs. The following Neumann condition is given at the center $r^* = 0$:

$$\frac{\partial^5 u^*}{\partial r^{*5}} = 0. \tag{8}$$

The cylindrical coordinate system was used in the present study, and the calculation of flow velocity on the central axis could not be carried out. So the fourth order polynomial function (8) was used to obtain the central value of u^* by an extrapolation method (the fifth derivative was tested as an optimal value between the accuracy and the computational time).

Since in the present numerical analysis the explicit formulation (time marching convergence procedure) was adopted in HSMAC method, time step Δt is limited for the numerical convergence and $\Delta t = 1.0 \times 10^{-5}$–$1.0 \times 10^{-3}$ were used to meet the following convergence criteria:

$$|\varepsilon| < 1.0 \times 10^{-4}, \quad \varepsilon = \frac{\zeta^{n+1} - \zeta^n}{\zeta^n}, \tag{9}$$

where ζ represents u^*, v^*, w^*, and p^* in whole calculation domain and n represents time. It should be mentioned that the calculation was terminated when the velocity $\boldsymbol{v}^*$ at P_1, P_2, P_3, and P_4 locations become periodic (at the steady flow, the amplitude of periodic velocity is zero). Namely, the amplitude of the oscillation of velocity field at each given point did not change with time.

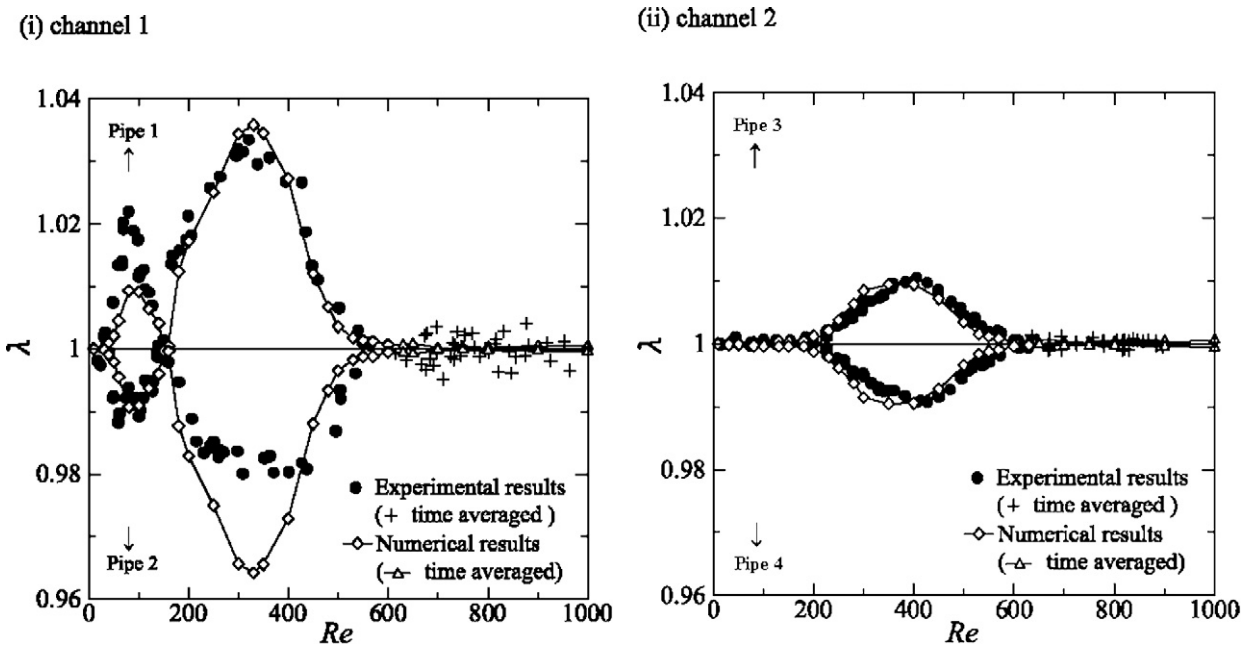

Fig. 4. Flow rate ratio vs. Reynolds numbers.

4. Results and discussions

4.1. Flow rate distribution

In order to characterize the hydrodynamic behavior of the cylindrical distributing channel, the flow rate distribution ratio λ is defined as the ratio of flow rate between two outlet branch pipes, $\lambda = q_1/q_2$ for channel 1 and $\lambda = q_3/q_4$ for channel 2, where q_1, q_2, q_3 and q_4 are the flow rate from two outlet branch pipes as shown in the horizontal planes of Fig. 2 (i) and (ii).

In Fig. 4 (i) channel 1 and (ii) channel 2, λ versus Reynolds number is displayed for $Re \leqslant 1000$ within the range of present study, where data obtained in the experiments are compared with the numerical results. The Reynolds number range was chosen in this study to include the steady state flow regime (including steady state symmetric flow and steady state asymmetric flow) and unsteady (time-dependent periodic) flow regime, which was particularly important in highly viscous fluid flows as often seen in chemical plants, processing plants and bio-medical flows et al. As indicated in Fig. 4(i), there exist two major regions of λ variation. First distinct region of λ, where deflection of flow rate distribution to either outlet branch pipe (the flow rate deflection) occurred, can be seen in the range of Reynolds number, $40 \leqslant Re \leqslant 150$. The maximum flow rate deflection occurred at approximately $Re \approx 80$, where the magnitude of λ was $\lambda = 1.009$ for pipe 1 and $\lambda = 0.991$ for pipe 2 from numerical results, while in experiment λ tends to deviate towards the outlet branch pipe 1, showing higher deflection results than the numerical results. It is seen that for the deflection to the outlet branch pipe 2 the numerical value tends to give good estimate to the experimental data (that is, the same probability deflection is seen in the numerical simulation) as seen in Fig. 4(i). Second distinct region of λ of the flow rate deflection was observed in the Reynolds number of $160 \leqslant Re \leqslant 550$, not only from experiment data, but also numerical results. The maximum deflection λ occurred at $Re \approx 330$ and the magnitude of the deflection λ was largely greater than the first region, i.e., $\lambda = 1.035$ for pipe 1 and $\lambda = 0.965$ for pipe 2 from numerical results. In the experiment data tended to show more deflection towards the outlet branch pipe 1 (although there was good agreement between the numerical results and experimental data for the outlet branch pipe 1 in the second distinct region, $160 \leqslant Re \leqslant 550$) while for the outlet branch pipe 2 the experimental data has a trend of reading lower values than that of numerical results. It should be emphasized that in experiments and numerical results, the deflection towards each outlet branch pipe occurred with the same probability (in the present study, for the steady state flow regime, "the same probability" means that on changing the Reynolds number and restarting the experiment there is equal probability of the flow deflection being toward either pipe. For the unsteady flow regime, it means that

λ oscillates back and forth with equal time spent at pipe 1 and pipe 2 or pipe 3 and pipe 4), although the magnitude of λ is different for pipe 1 and pipe 2. In the numerical analysis, the deflection phenomena were also dependent upon the Reynolds number, but occurred evenly to both outlet branch pipe with the same order of magnitude of λ (not only including the steady flow regime, but also time dependent periodic flow regime). This is because no matter how precise for the experimental setup and for keeping experimental conditions constant there exists a certain amount of error of tolerance, which reflects the major deviation of λ for pipe 1 and pipe 2 in the experimental data. Those were approximately maximum 2.1% in the first flow rate deflection region towards pipe 1 and 3.3% in the second flow rate deflection region towards pipe 1. However, in spite of some difference between numerical results and experimental data, the general trend shows a good agreement, as seen in Fig. 4(i).

In the same manner, in Fig. 4(ii), λ $(= q_3/q_4)$ versus Reynolds number are displayed for $Re \leqslant 1000$ within the range of present study. As indicated in Fig. 4(ii), there exists only one distinct region of λ variation in the range of Reynolds number, $180 \leqslant Re \leqslant 600$. The maximum flow rate deflection occurred at approximately $Re \approx 400$, where the magnitude of λ was 1.009 for pipe 3 and 0.991 for pipe 4 from numerical results, while in experiment λ was 1.01 for pipe 3 and 0.99 for pipe 4. The relative error of λ between numerical result and experimental value was approximately 0.1%. In comparison with channel 1 and channel 2, it was clearly shown that the magnitude of maximum λ for channel 2 is approximately the same as that of the first distinct region for channel 1. From general trend of λ in pipe 3 and pipe 4, the flow rate deflection for outlet pipes is moderate for channel 2, that is, when the outlet pipe distance is kept apart from the center line of the test section. This is because of small deflection of net swirl flow (caused by the circumferential velocity component v^* on r–θ plane) at the abruptly expanded part, and that will be described later in more detail. From the viewpoint of the engineering importance channel 2 can stably distribute the working fluid for both outlet pipes with smaller deflection of flow rate rather than channel 1, and is more suitable for the purpose of equal distribution. In addition, in the present study, for $Re \leqslant 630$, the steady state flow persists. For $630 \leqslant Re \leqslant 1000$, an unsteady (time-dependent periodic) flow begin to occur. A detailed description of flow regimes depending on the Reynolds number can be seen in the Ref. [16]. But here it should be mentioned the Reynolds number range for steady flow ($Re \leqslant 630$) is the same for both pipe configurations.

4.2. Variation of flow patterns

In Figs. 5–7, representative flow patterns obtained from steady state visualization and numerical simulation results associated with the flow rate distribution (as described in Fig. 4) are displayed in the cylindrical branching channel, i.e. the test section. The flow in the test section is strictly three-dimensional so that presentation of the flow field information is limited and for the sake of clarity figures are divided, as (i) the horizontal plane, (ii) the vertical plane and (iii) the r–θ plane at representative axial position z^* in each figure. With this manner, in Figs. 5–7, the representative flow patterns are depicted for $Re = 100$ and $Re = 300$ at channel 1 and $Re = 400$ at channel 2 respectively, which are representative Reynolds numbers associated with the distinctive regimes in the flow rate deflection characteristic in Fig. 4.

In Fig. 5, flow at Reynolds number, $Re = 100$ is presented, where the first flow rate deflection region ($40 \leqslant Re \leqslant 150$) for channel 1 was observed. As clearly seen in Fig. 5 (i) and (ii), the corner vortex region expands its size towards the down stream in the abruptly expanded part, distinct flow deflection occurs and the corner vortex also tends to go into breakdown, due to the vortex expansion. Large flow deflection on the vertical plane, Fig. 5(ii) is evident compared to the flow on the horizontal plane. Higher degree of the swirl flow (velocity vector on r–θ plane) appeared, as can be observed in Fig. 5(iii), particularly at position $z^* = 6.5$ (b), and which resultantly shows strong asymmetric flow configuration on the vertical plane. (In r–θ plane, the asymmetry is very hard to identify since the absolute magnitude of velocity in the plane is very small in its nature. However, it is our observation that the asymmetry in r–θ plane is better identified near the center of the channel.) It is thus interesting to note that the swirl flow and strong asymmetric flow pattern in the vertical plane are correlated while in the horizontal plane the asymmetry of the flow pattern is not so strong. Consequently the flow rate deflection to either outlet branch pipe is largely dependent on the swirl flow appearing on r–θ plane as whole, which may basically be attributed to abrupt expansion characteristics of geometry structure and helical vortex breakdown.

As it was observed in the flow rate deflection in Fig. 4(i), the second flow rate deflection regime for channel 1 appeared in the Reynolds number range, $160 \leqslant Re \leqslant 550$. The representative flow states are depicted in Fig. 6 for Reynolds number, $Re = 300$. In this regime, $160 \leqslant Re \leqslant 550$, the general trend of flow field is such that the extended

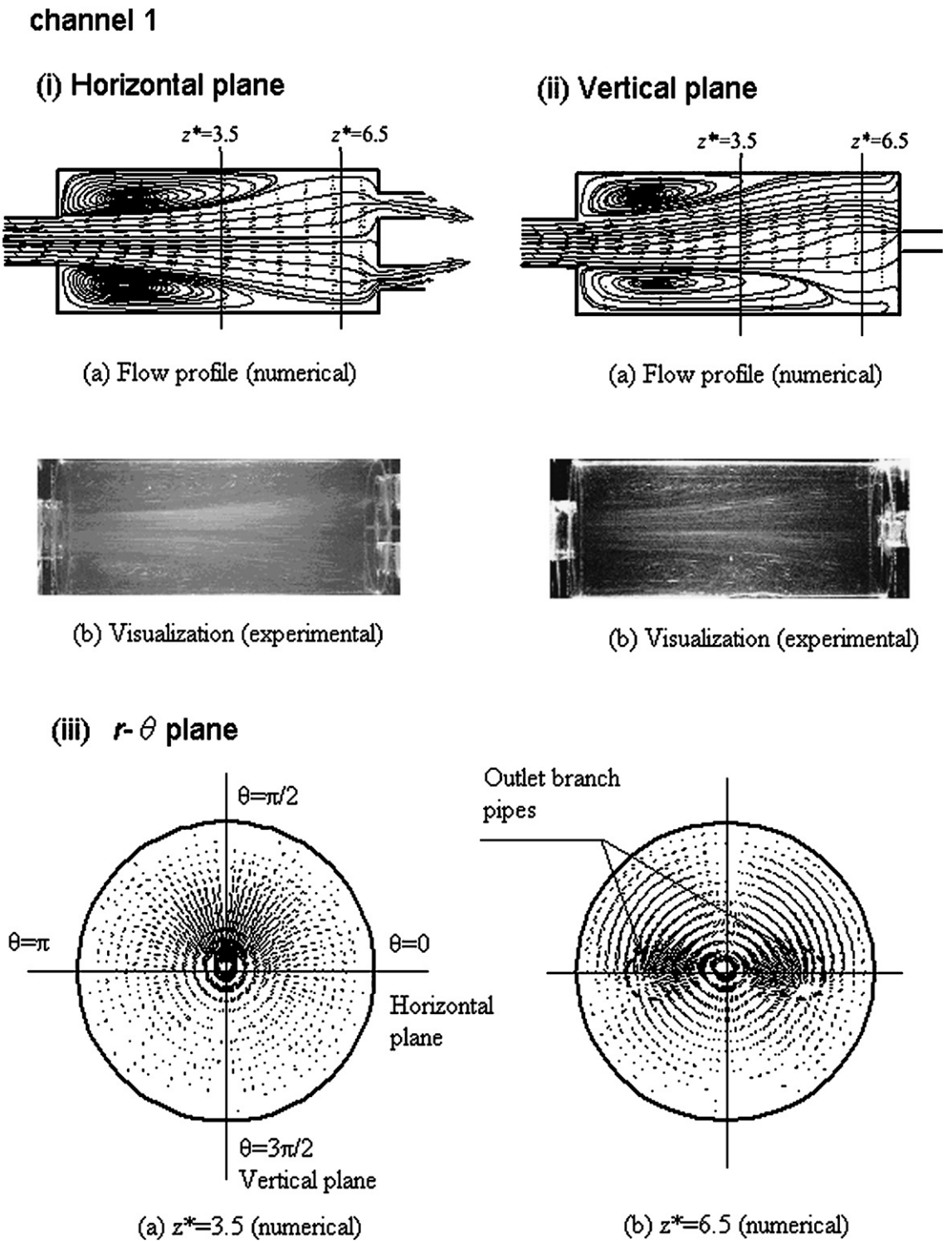

Fig. 5. Flow pattern; $Re = 100$, channel 1 (steady state flow regime); In the abruptly expanded part, the corner vortex region expands its size towards the down stream and distinct flow deflection occurs. Higher degree of the swirl flow appeared.

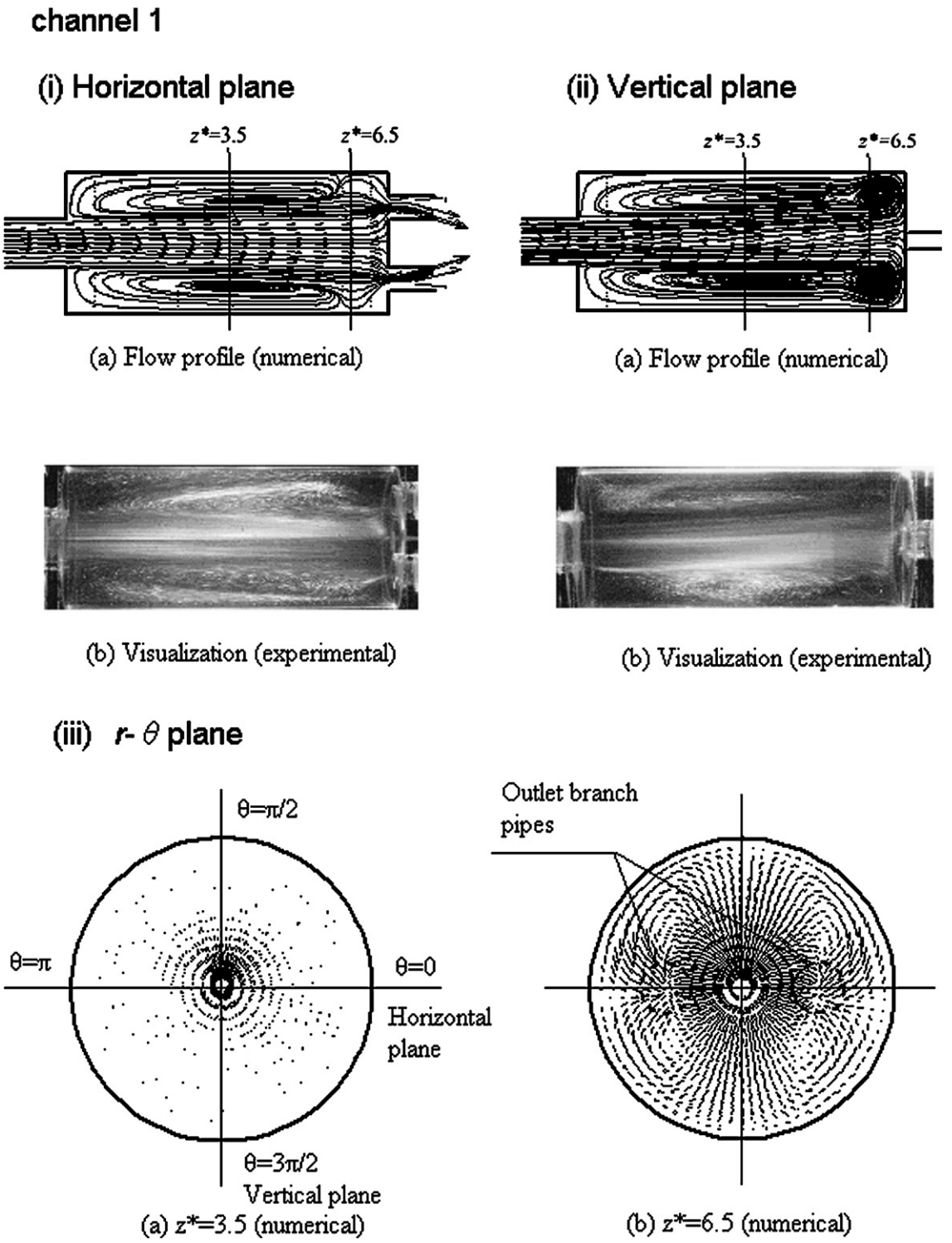

Fig. 6. Flow pattern; $Re = 300$, channel 1 (steady state flow regime); The extended corner vortex is further developed to the end wall and vortex breakdown occurs. The strong swirl flow is developed from upstream position.

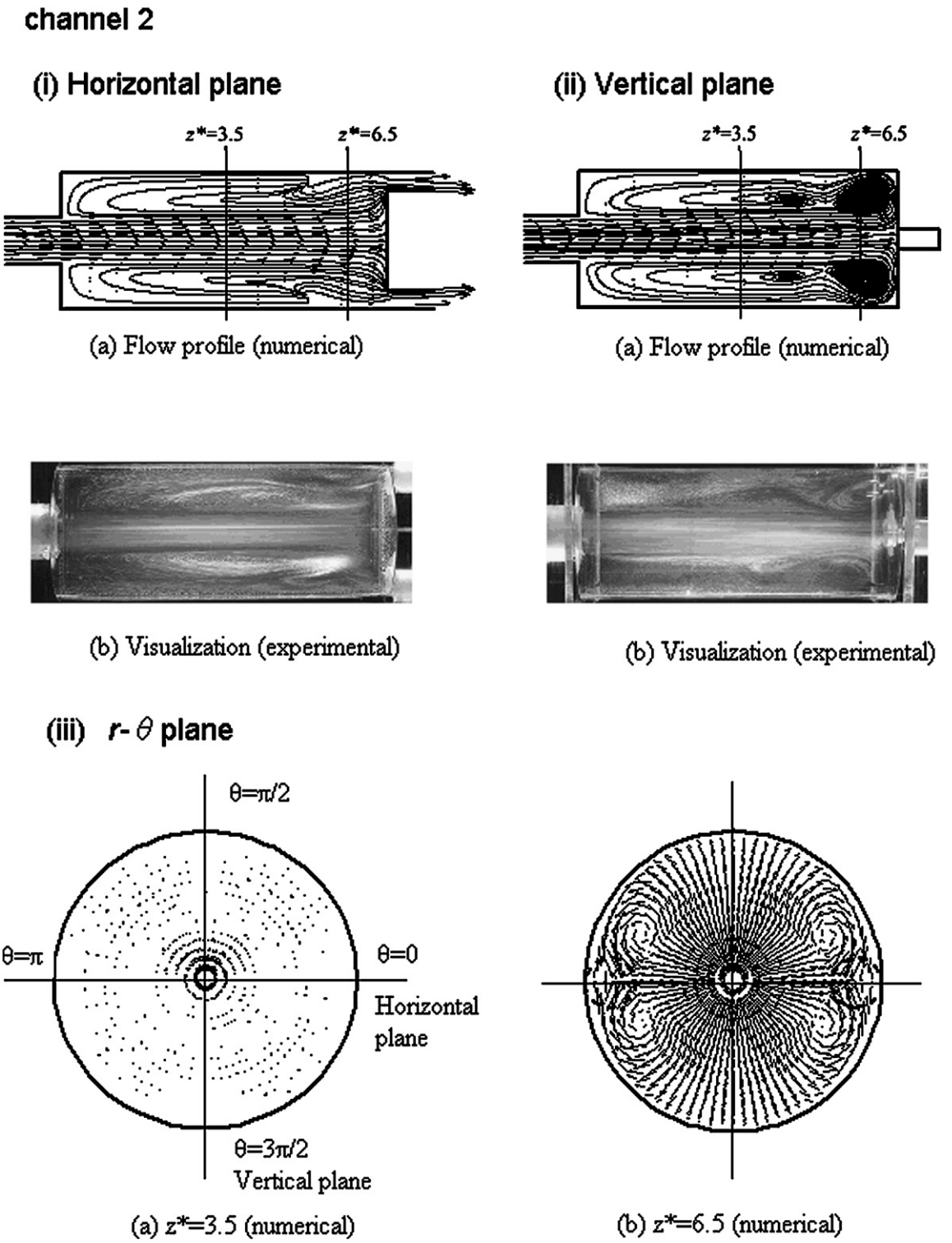

Fig. 7. Flow pattern; $Re = 400$, channel 2 (steady state flow regime); four vortex regions are generated in the extended corner vortex and the swirl flow at the end of the abruptly expanded part is further developed.

corner vortex is further developed to the end wall. Particularly as seen in Fig. 6(ii), on the vertical plane the secondary vortex region is generated in the extended corner vortex (the vortex breakdown occurs), where the re-attachment point of the corner vortex lies on the end wall in the vertical plane while in the horizontal plane the re-attachment point did not exist in the region, $160 \leqslant Re \leqslant 550$. Strong asymmetric flow pattern appears in the vertical plane, as seen in Fig. 6(ii) from both numerical result of flow profile (a) and the visualization result (b), and also in the horizontal plane, Fig. 6(i), fairly strong asymmetric flow pattern appears. Again in this second flow rate deflection region, $160 \leqslant Re \leqslant 550$, swirl flow appears, as seen in Fig. 6(iii) on the r–θ plane, particularly at positions $z^* = 6.5$ (b). This is probably due to existence of the extended corner vortex with newly generated secondary vortex region close to the end of the abruptly expanded part. The swirl flow is developed, as shown in Fig. 6(iii)(b), leading higher deflection of flow rate and thus higher λ in the second flow rate deflection region, compared with the first flow rate deflection region of $40 \leqslant Re \leqslant 150$.

In Fig. 7, flow at Reynolds number, $Re = 400$ is presented, where the flow rate deflection region ($180 \leqslant Re \leqslant 600$) for channel 2 was observed. In this regime, $180 \leqslant Re \leqslant 600$, as seen in Fig. 7(i), on horizontal plane the main flow extends close to the end of the abruptly expanded part. While in the vertical plane, as seen in Fig. 7(ii), four vortex regions are generated in the extended corner vortex and the re-attachment point of the corner vortex lies on the front of the abruptly expanded part in this regime, $180 \leqslant Re \leqslant 600$ (based on Figs. 5–7, with the Reynolds number increase, the corner vortex expands and goes into breakdown in the almost whole geometry). This is because the swirl flow at the end of the abruptly expanded part is further developed, compared with channel 1, which will be described later. Swirl flow appears, as seen in Fig. 7(iii) on the r–θ plane, particularly at position $z^* = 6.5$ (b) there exist distinct four vortex regions in r–θ plane (from Figs. 5(iii)–7(iii), it can be seen that swirl flow becomes stronger and stronger with the Reynolds number increase). It is shown that the flow rate deflection occurs, which correlated with swirl and helical vortex breakdown mode and similar phenomena can also be seen in Ref. [3,4]. However, in comparison with $Re = 300$ at channel 1, the flow rate deflection is decreased. Since the strongest flow deflection occurs when there is the strongest swirl, any mechanism/structure in the present channel configuration designed to inhibit swirl would also reduce flow deflection.

4.3. Interpretation of flow rate deflection characteristics in three-dimensional branching channel with sudden expansion

In order to relate the observation, Fig. 4, with one essential parameter, and to give an insight for the deflection characteristics, a numerical study was conducted in the present study. According to the obtained results in Section 4.2, it become clear phenomenologically that the flow states associated with the deflection characteristics are largely affected by the presence of swirl flow in the abruptly expanded part. Thus, to relate the deflection characteristics with parametric quantity, the following quantity is defined in the present study,

$$\Gamma_n = \frac{(1/V)\int_V v^* \,\mathrm{d}V}{W_{\max}}, \qquad \overline{\Gamma}_n = \frac{1}{t}\int_0^\infty \Gamma_n \,\mathrm{d}t \tag{10}$$

where Γ_n is defined as Swirl Ratio, which is the ratio between the axial representative velocity $W_{\max}$ and the volumetric average of the circumferential velocity component in the abruptly expanded part. V is the total volume of the abruptly expanded part. In case of the unsteady periodic flow, the time average of Γ_n is taken as defined $\overline{\Gamma}_n$ in formula (9). For Γ_n and $\overline{\Gamma}_n$, the numerical simulation was carried out for variation of Reynolds number within the limit in the present study. The calculation was performed to produce numerical solutions of flow field by varying Reynolds number, and for each given Reynolds number Γ_n and $\overline{\Gamma}_n$ were calculated from the resultant flow field. In Fig. 8(i) channel 1 and (ii) channel 2, results of the numerical simulation are depicted.

As seen in Fig. 8(i), there are two identical paths of Γ_n (and $\overline{\Gamma}_n$), depending upon net effect for the direction of θ of the circumferential velocity component, and the two paths occurred with the same probability for increment of Reynolds number as preciously described. There is the similarity between two profile of Γ_n and $\overline{\Gamma}_n$ in Fig. 8(i) and λ in Fig. 4(i). The first deflection regime, $40 \leqslant Re \leqslant 150$, and the second flow rate deflection regime, $160 \leqslant Re \leqslant 550$ (both are the steady state flow regimes and $Re \geqslant 630$ is the case of unsteady periodic flow), in Fig. 4(i) are well matched with the result of Γ_n in Fig. 8(i). Reynolds numbers, which gave maximum flow rate deflection λ in the first deflection region and in the second flow rate deflection region, $Re_1 \approx 80$ and $Re_2 \approx 330$ respectively in Fig. 4(i), are

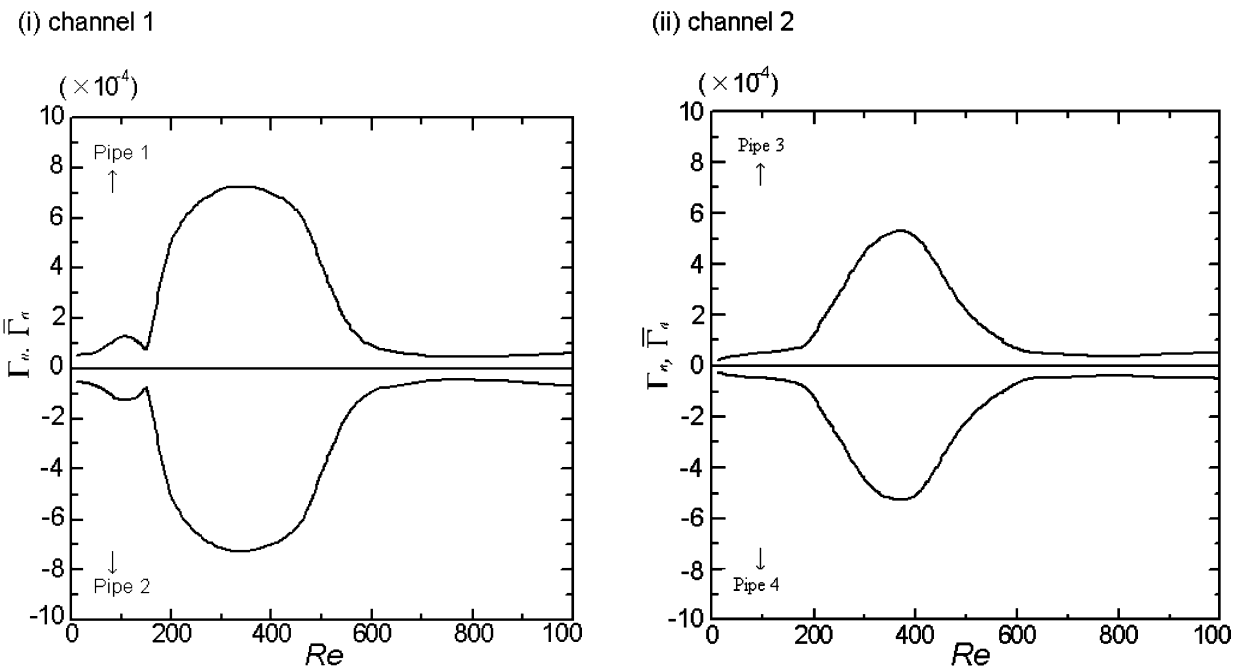

Fig. 8. Swirl rate ratio vs. Reynolds numbers ($Re \leqslant 630$, the steady state flow regime; $630 \leqslant Re \leqslant 1000$, an unsteady periodic flow).

also in good agreement with the associate Reynolds numbers for Γ_n shown in Fig. 8(i). Thus, according to the fact based on the comparison between λ and Γ_n, the net effect of the swirl flow, which is generated due to the nature of three-dimensional asymmetric configuration of the test section and affected by the existence of vortices, is the key factor to determine the characteristics of flow rate deflection in the benchmark model channel studied in the present investigation.

As indicated in Fig. 8(ii), there exists a major deflection region of Γ_n (and $\overline{\Gamma}_n$), and the deflection occurred with the same probability for increment of Reynolds number as preciously described. There is the similarity between the profile of Γ_n (and $\overline{\Gamma}_n$) in Fig. 8(ii) and that of λ in Fig. 4(ii). The deflection regime, $180 \leqslant Re \leqslant 600$, in Fig. 4(ii) are well matched with the result of Γ_n in Fig. 8(ii). Reynolds number, which gave maximum flow rate deflection λ in the flow rate deflection region, $Re \approx 400$ in Fig. 4(ii), is also in good agreement with the associate Reynolds number for Γ_n as shown in Fig. 8(ii). In comparison with channel 1, the deflection of Γ_n (and $\overline{\Gamma}_n$) becomes small. Consequently both the distinct region of λ of the flow rate deflection and the distinct value of λ of the flow rate deflection in channel 2 are decreased.

5. Conclusions

Flow rate deflection characteristics in a three-dimensional cylindrical branching channel were obtained by experimental measurements and numerical simulations.

There are two major regimes for channel 1 and only one distinct regime for channel 2, where the flow rate deflection occurs to either outlet branch pipe, magnitude depending upon the Reynolds number. In comparison with channel 1 and channel 2, both the region of the flow rate deflection and the distinct value of the flow rate deflection in channel 2 are smaller than that in channel 1. From the viewpoint of the engineering importance channel 2 can stably distribute the working fluid for both outlet pipes with smaller deflection of flow rate rather than channel 1, and is more suitable for the purpose of equal distributor.

Detailed flow states were presented associated with the flow rate deflection characteristics, showing flow patterns on representative planes in the abruptly expanded part. It was found that in general the weakly asymmetric flow patterns in the horizontal plane are well kept for the entire range of Reynolds numbers in the steady state regime, while in the vertical plane there appeared strong asymmetric flow patterns. This was chiefly related with the strong deviation of swirl flow (on the r–θ plane) to the horizontal plane and it was found that the existence of swirl flow,

appearing on the r–θ plane, plays an important role to determine the state of flow field and in turn affects the flow rate deflection characteristics.

Based on the results gained from the flow field phenomena, the parametric quantity defined as the Swirl Ratio showed excellent predictability for the flow rate deflection characteristics, and indicated that the net swirl generated in the flow field determines the overall character of the flow rate deflection to the outlet branch pipes independent of the flow mode. In comparison with channels 1 and 2, the deflection of the Swirl Ratio for channel 2 becomes small. Consequently both the region of the flow rate deflection and the distinct value of the flow rate deflection in channel 2 are decreased.

Acknowledgements

This work was carried out in collaboration with Project Research in Advanced Fluid Information Research Center, Tohoku University. Major part of numerical simulation was performed by ORIGIN 2000 in the center. This work was also partly supported by a grant to FRONTIER (Zero-Emission project) at Doshisha University from the Ministry of Education, Culture, Sports, Science and Technology, Japan.

References

[1] A.S. Joseph, E.F. Allen (Eds.), Handbook of Fluid Dynamics and Fluid Machinery 3, Wiley, 1996, pp. 2005–2018.
[2] D. Liepsch, An introduction to biofluid mechanics – basic models and applications, J. Biomech. 35 (2002) 415–435.
[3] T.M. Liou, T.W. Chang, W.C. Chang, Pulsatile flow through a bifurcation with a cerebrovascular aneurysm, J. Biomech. Eng. 116 (1994) 112–118.
[4] T.M. Liou, W.C. Chang, C.C. Liao, Experimental study of steady and pulsatile flows in cerebral aneurysm model of various sizes at branching site, J. Biomech. Eng. 119 (1997) 325–332.
[5] W. Cherdron, F. Durst, J.H. Whitelaw, Asymmetric flows and instabilities in symmetric ducts with sudden expansions, J. Fluid Mech. 84 (1) (1978) 13–31.
[6] J. Mizushima, Y. Shiotani, Structural instability of the bifurcation diagram for two-dimensional flow in a channel with a sudden expansion, J. Fluid Mech. 420 (2000) 131–145.
[7] R.M. Fearn, T. Mullin, K.A. Cliffe, Nonlinear flow phenomena in a symmetric sudden expansion, J. Fluid Mech. 211 (1990) 595–608.
[8] N. Alleborn, K. Nandakumar, H. Raszillier, F. Durst, Further contributions on the two-dimensional flow in a sudden expansion, J. Fluid Mech. 330 (1997) 169–188.
[9] T. Hawa, Z. Rusak, The dynamics of a laminar flow in a symmetric channel with a sudden expansion, J. Fluid Mech. 436 (2001) 283–320.
[10] F. Durst, A. Melling, J.H. Whitelaw, Low Reynolds number flow over a plane symmetric sudden expansion, J. Fluid Mech. 64 (1974) 111–128.
[11] H.J. Sheen, W.J. Chen, J.S. Wu, Flow patterns for an annular flow over an axisymmetric sudden expansion, J. Fluid Mech. 350 (1997) 177–188.
[12] J. Mizushima, H. Takahashi, Transitions of flow in a distributor cavity with one inlet and two outlets, J. Phys. Soc. Japan 68 (11) (1999) 3514–3519.
[13] J. Mizushima, T. Inui, Transitions of three-dimensional flow through a rectangular duct with a suddenly expanded and contracted part, J. Phys. Soc. Japan 70 (5) (2001) 1171–1174.
[14] C.W. Hirt, B.D. Nichols, N.C. Romero, SOLA-A Numerical solution algorithm for transient fluid flows, Wiley Eastera Limited, Los Alamos Scientific Laboratory report, LA-5852, 1975.
[15] S.T. McComas, Hydrodynamic entrance lengths for duct of arbitrary cross section, Trans. ASME 89 (1967) 847–850.
[16] H. Yamaguchi, A. Ito, M. Kuribayashi, X.R. Zhang, H. Nishiyama, An experimental study on the flow characteristics in a three-dimensional cylindrical branching channel, Flow Measurement and Instrumentation 16 (2005) 241–249.